FLOW LOSS AND FLOW STRUCTURE OF CIRCULAR ARC CASCADES WITH DIFFERENT LEADING AND TRAILING EDGES

Tao BIAN[1], Christian LANDFESTER[2], Jun FENG[1],
Qianpeng HAN[3], Martin BÖHLE[2]

[1] *Jianghan University, Institute for Interdisciplinary Research, 430056 Wuhan, China*

[2] *Technical University of Kaiserslautern, Institute of Fluid Mechanics and Fluid Machinery, 67663 Kaiserslautern, Germany*

[3] *Jianghan University, School of Electromechanical and Architectural Engineering, 430056 Wuhan, China*

SUMMARY

Due to the much lower cost of production, circular arc blades with flat leading and trailing edges are often applied to axial flow fans as guide vanes. However, the flat leading and trailing edge of the blade may also cause relatively higher flow loss. At present, there is few available information in the open literature focusing on the circular arc blade, especially the influence of the leading edge geometry on the aerodynamic performance of the blade. In this study two kinds of circular arc blades with different leading and trailing edges are investigated by numerical and experimental methods to compare the flow loss and flow structure between them. The flow structure of both blades is illustrated based on numerical and experimental oil-pictures.

INTRODUCTION

Compared with circular arc blade with rounded leading and trailing edges, the circular arc blade with flat leading and trailing edges has lower cost of production but also relatively higher flow loss. At present, there is a few available information in the open literature focusing on the circular arc blade. In particular, the influence of leading and trailing edge geometry on the flow loss and flow structure remains unknown. Therefore, two questions are raised: Firstly, how large is the flow loss and flow turning angle of circular arc blade for different operating conditions. Secondly, how much is the influence of the leading and trailing edge geometry on flow loss and flow structure.

Most researches on circular arc blade are based on theory of Weinig [1], who has developed an analytical theory based on potential flow for cascades consisting of thin cambered blades. John et al. [2] have examined the transonic flow around a circular arc blade with Reynolds number from 1×10^6 to 17×10^6. A design method for cascades consisting of circular arc blades with constant thickness has been developed [3], it is based on a singularity method combined with a CFD-data-based flow loss model.

Suzuki *et al.* [4] have investigated the total pressure loss coefficient of thin circular arc blades for different camber angles. Suzuki's work shows that the result of CFD simulation is sufficiently useful when the camber angle of the circular arc blades is below about 49.5 ^{o}. According to his result, the camber angle of the investigated blades in this study is chosen as $\varphi = 20$ ^{o}.

A comparison between NACA 65 profiles and circular arc blades for different spacing ratios, Reynolds numbers and incidences has already been made, the result of the comparison indicates that the main reason of the higher losses of circular arc blades is the separation bubbles induced by the leading edge of the blade [5]. The leading edge geometry of circular arc blades has a significant influence on the flow loss.

In this study two kinds of circular arc blades with different leading and trailing edges are examined by numerical and experimental methods. The influence of the sidewall on the flow loss and flow structure is taken into account. The research purposes of this study are: Firstly, flow loss and turning angle of both investigated blades is investigated for different incidence angles, so the performance of each blade can be compared. Additionally, by comparing the flow loss and turning angle of both investigated blades, the influence of the leading edge geometry on the flow loss and turning angle is detected. Secondly, the flow structures on the sidewall of both investigated blades are illustrated on the basis of numerical and experimental oil-flow picture. Therefore, the influence of the leading edge geometry on the flow structure can be investigated and discussed. Finally, the flow loss on the measuring plane is investigated, so the three-dimensional flow structure on the measuring plane, especially in the corner area between the blade and the corresponding sidewall, is detected.

THE INVESTIGATED BLADES

Both investigated blades are circular arc blade with constant thickness. Blade A has rounded leading and trailing edges, the leading and trailing edges of blade B are flat (Fig. 1). Both blades have a chord length l of 100 mm and a camber angel φ of $\varphi = 20$ ^{o}. The stagger angle λ is set as 30 ^{o}. The investigated spacing ratio t/l is 1.0. The Reynolds Number is $Re = 4 \times 10^5$. All examinations were performed for variant incidence angles from $i = -15$ ^{o} to $i = 10$ ^{o} with a stepwise movement of 5 ^{o}. Fig. 2 shows the nomenclature of both investigated blades is shown, and table 1 shows the parameters of the blades.

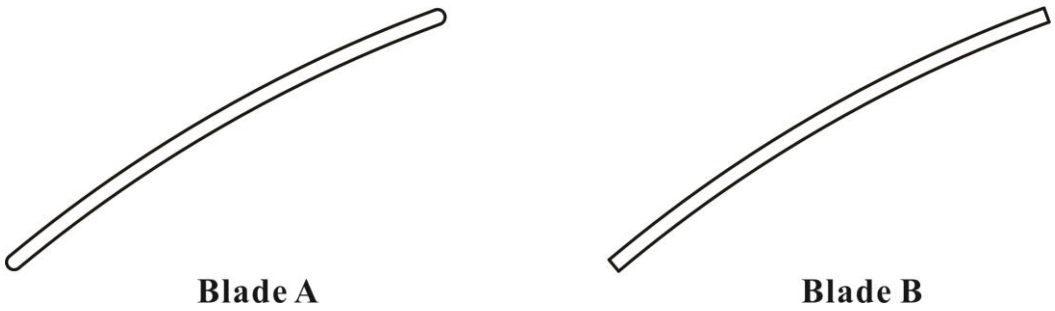

Figure 1: the investigated blades

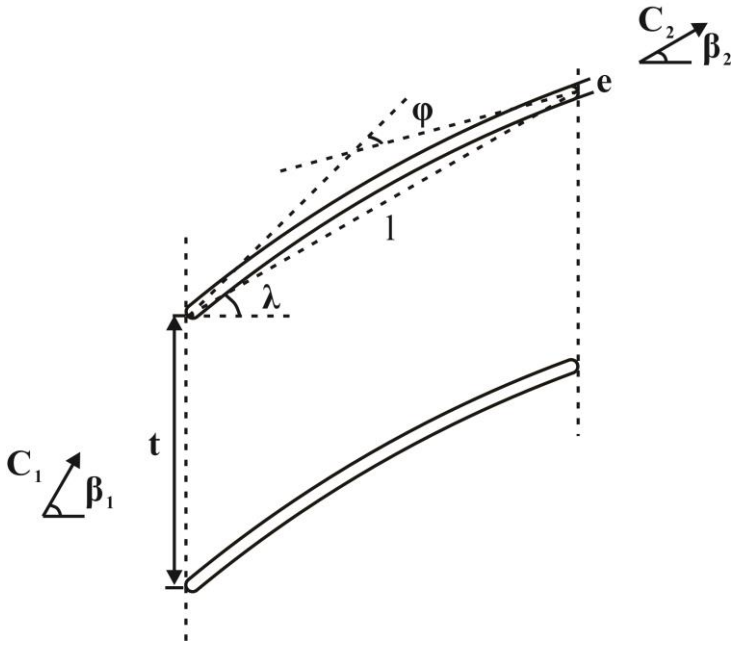

Figure 2: the nomenclature of the investigated blades

Table 1: parameters of the investigated blades

	Blade A	**Blade B**
l/ mm	100	100
φ/ º	20	20
λ/ º	30	30
e/l	0.03	0.03
b/l	2	2
t/l	1.0	1.0
Leading and trailing edge	rounded	flat

NUMERICAL INVESTIGATION

The CFD simulations were conducted with software Fluent 15.0. Reynolds-Averaged Navier-Stokes equations (RANS) were solved on an unstructured grid. A second order finite volume-discretization was applied to a collocated grid. The transition SST model was selected as turbulence model, which is commonly used for airfoil flow. The transition SST turbulence model is based on the coupling of Menter K-ω SST model transport equations with two other transport equations for intermittency and transient onset criteria. Menter K-ω SST model consists of a transformation from K-ε model to K-ω model in wall-near areas and the standard K-ω model in free-stream areas [6]. Therefore, the transition SST model gains major advantages of both K-ε model and K-ω model in the prediction of flow behavior.

Using the software package Icem CFD from Ansys 15.0, the three-dimensional flow domains were discretized with block structured grids for both investigated blades. In order to determine the flow behavior of the boundary layers, the grids have been refined continuously towards the walls. The maximum spacing of the meshes to the walls is smaller than 0.01 mm, so that the y^+ is smaller than 1. A three-dimensional mesh consists of about 4 million cells. Fig. 3 shows the details of the grid.

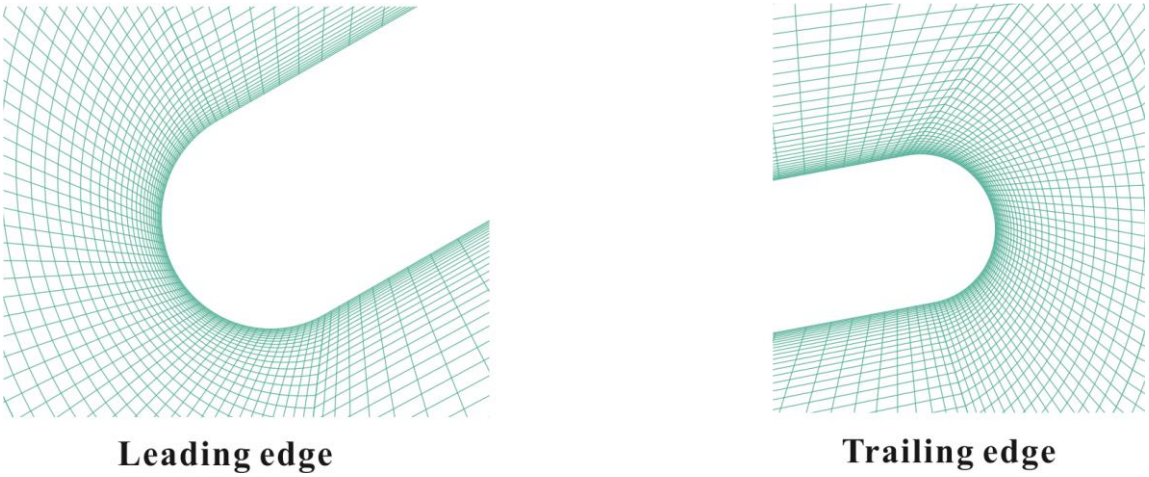

Figure 3: the grid details

The numerical investigations are performed at Reynolds Numbers of 4×10^5. The Reynolds number is defined by:

$$\mathrm{Re} = \frac{\rho * l * C_1}{\mu} \tag{1}$$

Here ρ is the density of fluid, l is the chord length of blade, C_1 is inflow velocity, and μ is dynamical viscosity.

In order to consider the influence of the boundary layer on the sidewall, the velocity profile of the incoming flow has been investigated based on the free-flow measurement in the wind tunnel, which is used in the experimental investigations. The velocity profile has been implemented in the inlet boundary conditions with a UDF (User Defined Function). Fig4 depicts the used velocity profile. Here, δ is the thickness of the boundary layer of the sidewall on the inlet, which is measured by the wind tunnel. x is the distance between the current position and the sidewall in the blade height direction (in this work is in x-direction). C_{max} is the maximum velocity at the outer edge of the boundary layer of the sidewall.

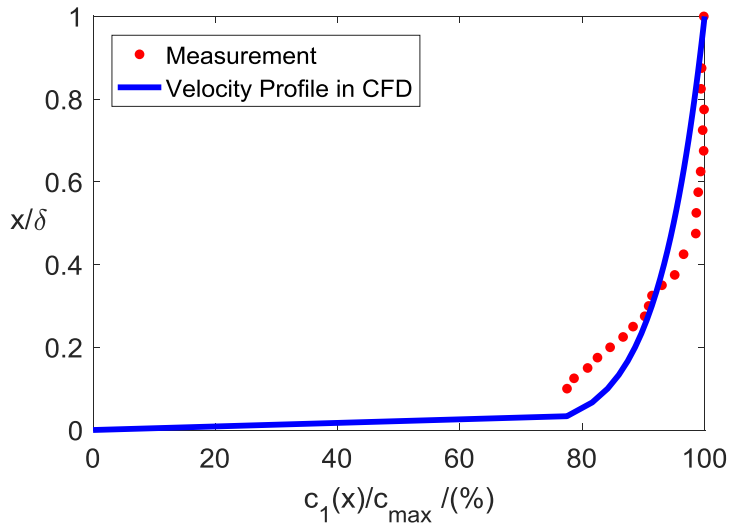

Figure 4: flow domain with boundary condition

The Mach number of the inflow is Ma < 0.3, which characterizes an incompressible inflow. Furthermore the assumptions of isothermal and steady state conditions were made. So the energy equation was not needed and no boundary condition for the temperature was set. The turbulent intensity T_u was set as 2% and the turbulent length scale was 0.07 × 0.2 m (height of the blade) =

0.014 m [7]. All examinations were performed for the incidence angles from i = −15° to i = 10° with a stepwise movement of 5°. The plane for computing the results is 50 mm downstream from the trailing edge of the blade. Fig. 5 illustrates the flow domain with boundary conditions. The boundary conditions at each surface are listed in Table 2.

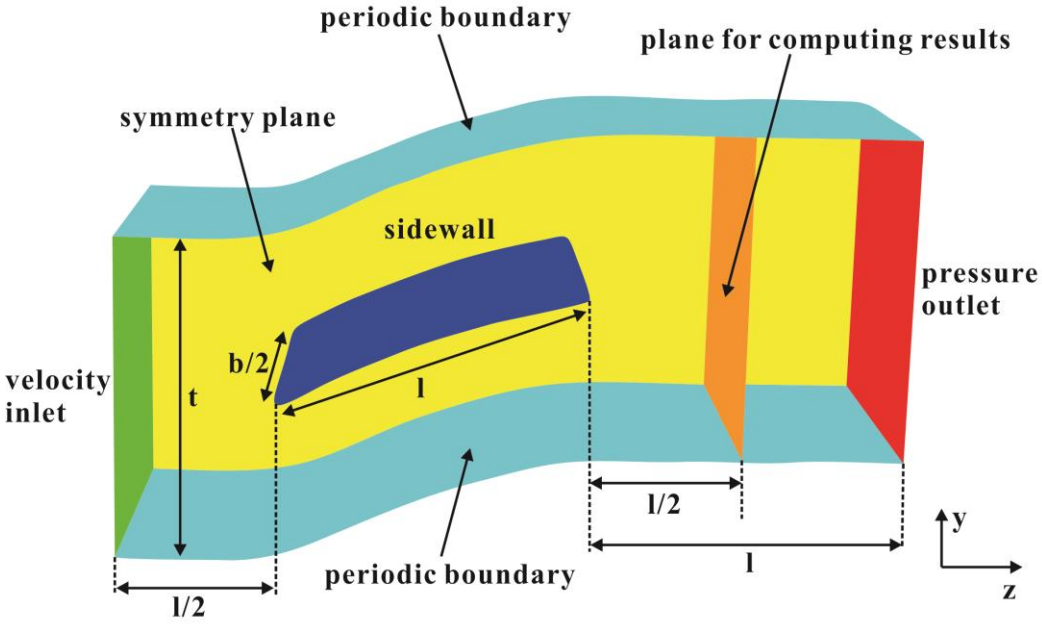

Figure 5: flow domain with boundary condition

Table 2: boundary conditions on each surface

Surface	Boundary conditions
inlet	velocity inlet with UDF
outlet	pressure outlet
periodic boundary	periodic
symmetry plane	symmetry
sidewall	non-slip wall

EXPERIMENTAL INVESTIGATION

The experimental investigations were conducted in a wind tunnel, which consists of an inlet nozzle, an axial compressor, a honeycomb rectifier, an acceleration nozzle and a measuring section. The inlet nozzle has an inner diameter of 710 mm and a length of 1575 mm. Next to the inlet nozzle are two axial compressors, each axial compressor is controlled by a frequency converter and has the power up to 18.5 kW. The honeycomb rectifier is used to reduce the swirled flow from the axial compressor. After the honeycomb rectifier, the flow goes through the acceleration nozzle to reduce velocity differences and forms a unified velocity distribution on the measuring section, which is located at the end of the wind tunnel (s. Fig. 6).

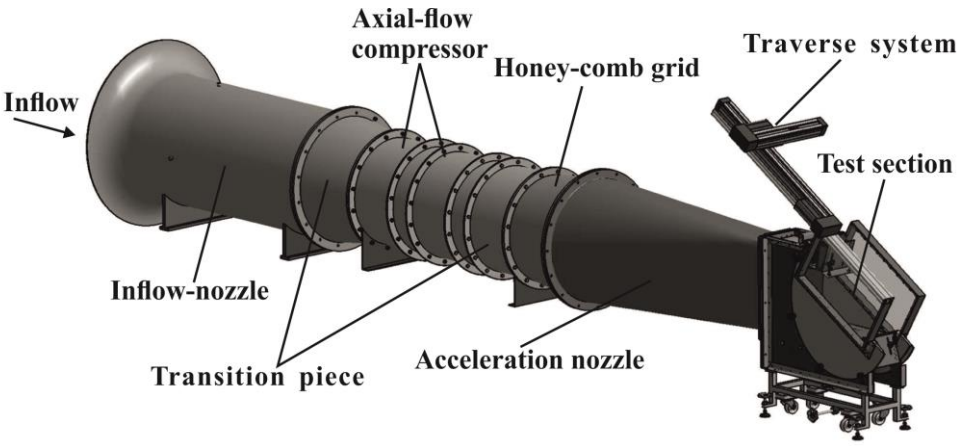

Figure 6: wind tunnel

The total pressure and dynamic pressure of the inflow are measured by a Prandtl probe, which is located in the center of inflow section (s. Fig.7). The total pressures on the measuring plane is measured by the five-hole probe, which is mounted on the traverse system. With this traverse system the five-hole probe can be moved in both x- and y- directions by step motors, so the five hole probe can measure the pressures of any point on the measuring plane. The investigated blades are mounted in two transparent Plexiglas plates, therefore the experimental oil-flow picture of the flow structure can be realized.

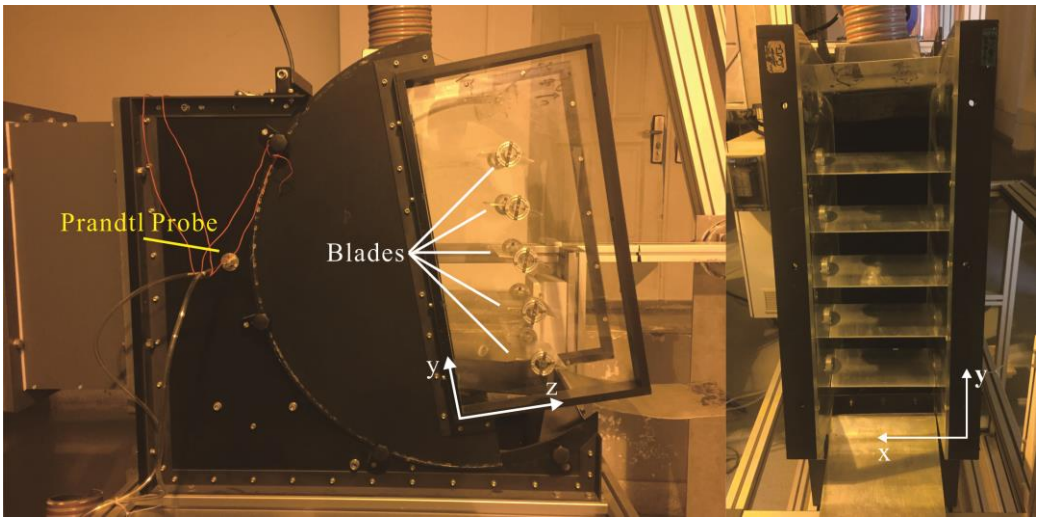

Figure 7: wind tunnel and measuring section

Two side channel compressors are mounted on the top and bottom of the measuring section. Each side channel compressor is controlled by a frequency converter and has a power up to 12.5 kW. The function of both side channel compressors is to ensure that the boundary layer on the upper and lower wall is sucked out so that the inflow becomes periodic in y-direction.

RESULTS AND DISCUSSION

Loss coefficient and turning angle

The dimensionless loss coefficient ζ and turning angle $\Delta\beta$ of the blades are investigated for different incidences (s. Figs. 8 and 9). The loss coefficient ζ is defined by:

$$\zeta = \frac{P_{tot,1} - P_{tot,2}}{\frac{1}{2} * \rho * C_1^2} \qquad (2)$$

Here $P_{tot,\,1}$ and $P_{tot,\,2}$ are the mass-averaged total pressures on inlet and measuring plane. C_1 is the velocity on the inlet.

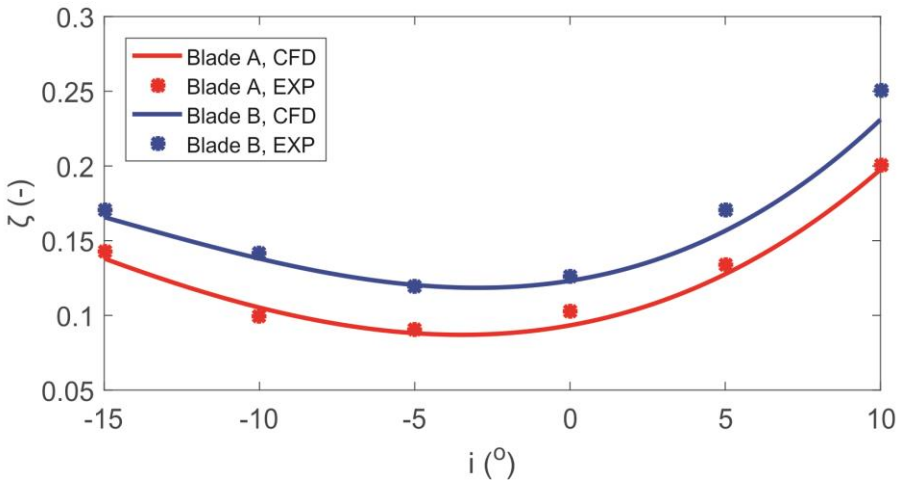

Figure 8: flow loss of the investigated blades

As the results show the numerical loss coefficients have a relative good agreement with the experimental results. In general, blade B has a higher flow loss than blade A. The lowest flow loss of both investigated occurs at incidence i = -4°.

The outflow angle β_2 and the resulting turning angle $\Delta\beta$ are defined as:

$$\tan\beta_2 = \frac{C_{2y}}{C_{2z}}, \qquad \Delta\beta = \beta_1 - \beta_2 \tag{3}$$

Here β_2 is flow angle on measuring plane, C_{2y} and C_{2z} are the mass-averaged velocity on the measuring plane in y-direction and z-direction. β_1 is the inflow angle. As Fig. 9 shows, the difference of the turning angle between blade A and blade B is small.

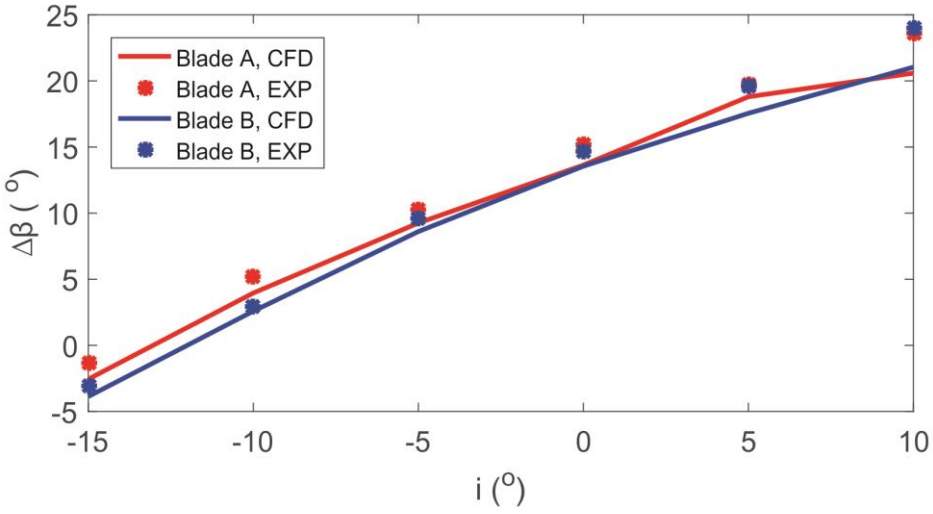

Figure 9: turning angle of the investigated blades

Loss distribution on the measuring plane

In order to determine the three-dimensional flow structure in the corner between the blade and the corresponding sidewall, the loss distributions of both investigated blades are depicted in Figs. 10 and 11. The loss distribution is investigated on the plane, which is parallel to the inflow plane and 50 mm downstream behind the trailing edge of the blade. The results of numerical and experimental loss distributions have relative good agreement.

Due to the friction, the velocity close to the sidewall and blade slows down, which leads to the lower total pressure near the sidewall and blade and higher flow loss. Therefore, it is typical that the high loss coefficient generates in the region which is near the sidewall and blade, especially in the corner between them.

For i = -5 °, the secondary flow is still weak, the primary flow is strong enough to stop the area of high losses from moving to the middle of the wind tunnel, so the area of high losses near the sidewall is still small and a large area of low constant flow losses (i.e the wake behind the blade) takes place between the sidewalls.

When i increase to 5 °, the secondary flow and the flow separation on the blade is stronger, thus the wake behind the blade thickens, and the area of high losses near the sidewall becomes larger.

Due to the flat leading edge, the flow separation of blade B is more strongly than blade A. So blade B has a larger wake behind the blade than blade A, which leads to a higher flow loss of blade B (Fig. 11).

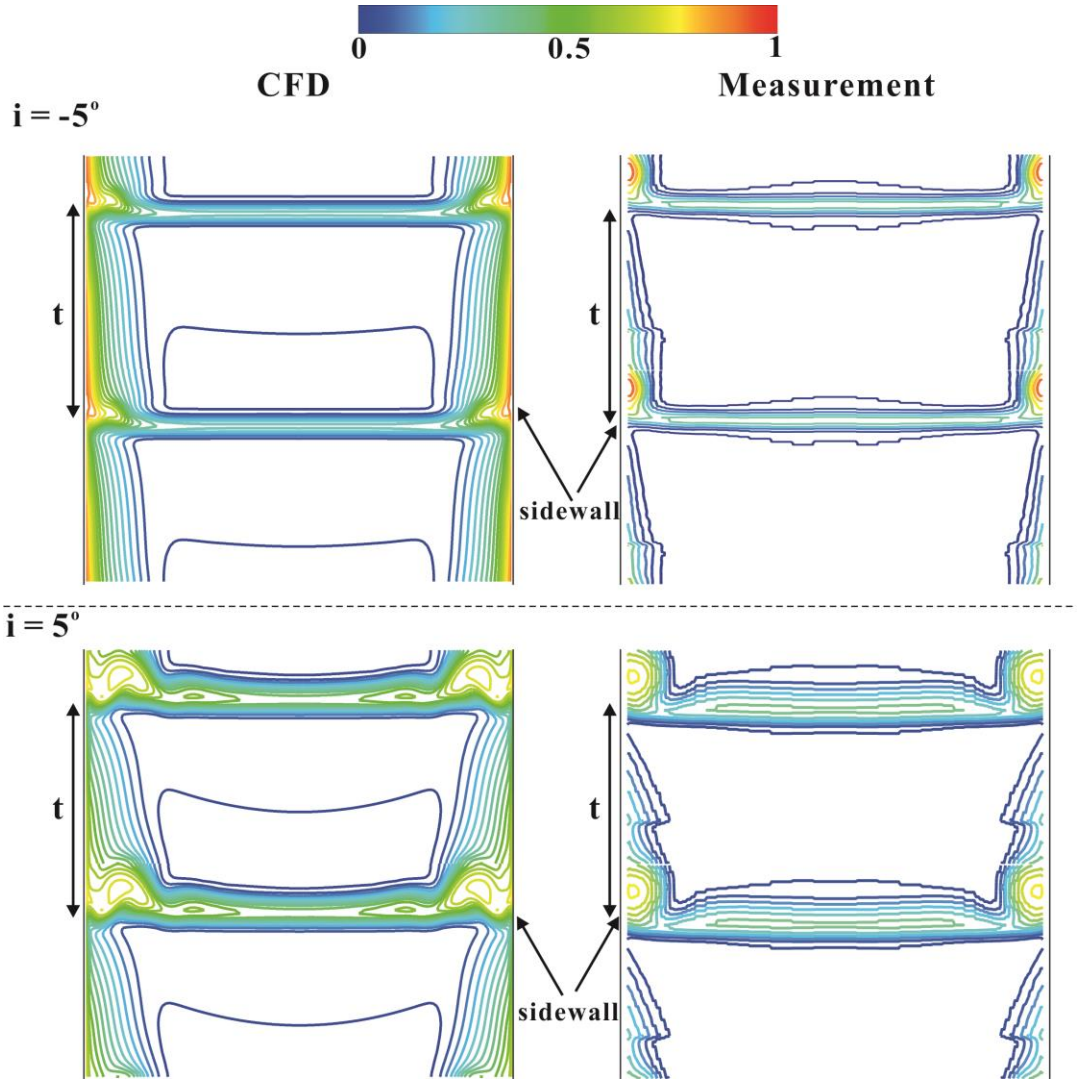

Figure 10: loss distribution on the measuring plane of blade A

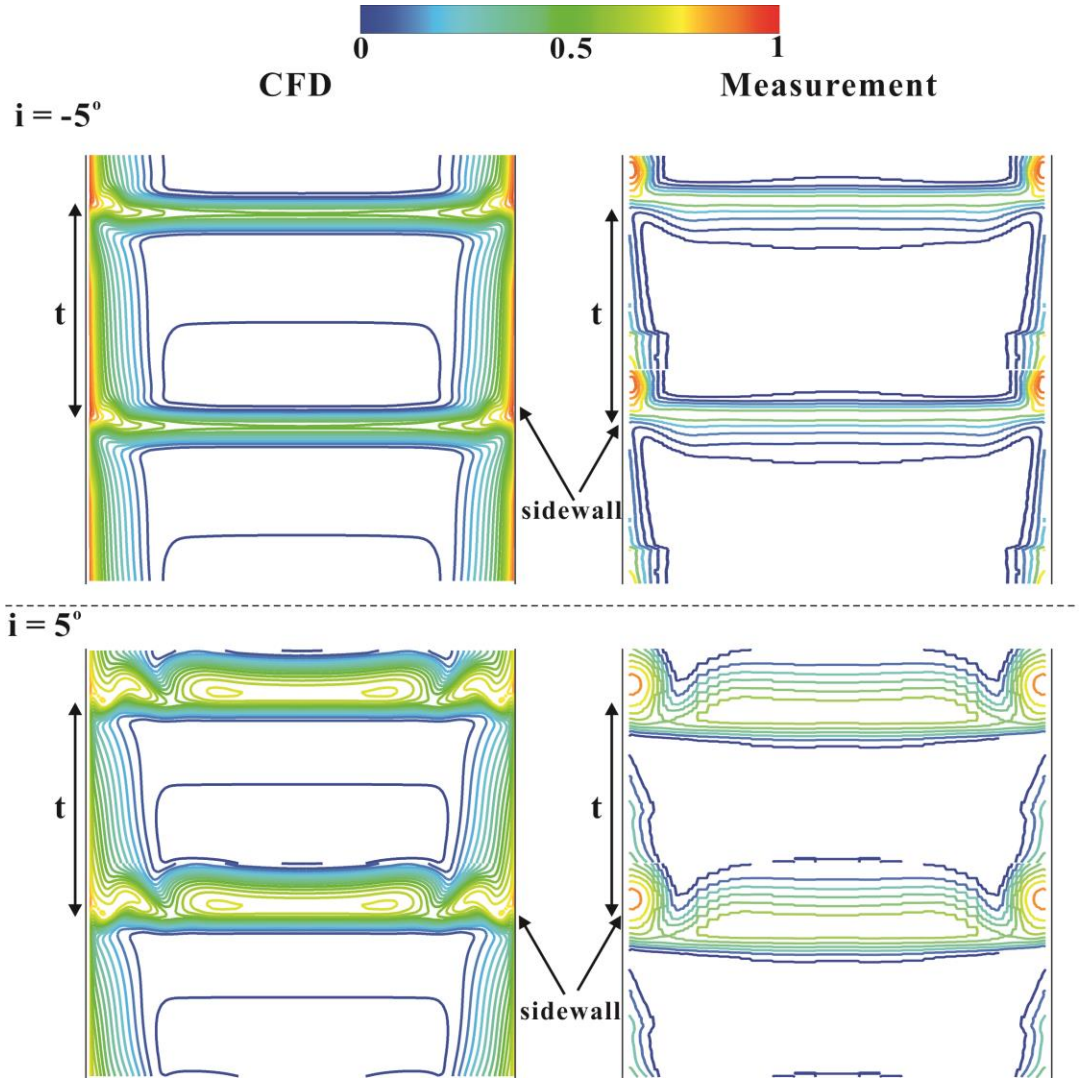

Figure 11: loss distribution on the measuring plane of blade B

Flow structure on the sidewall

The flow structures of both investigated blades are depicted in Figs. 12 to 15. The experimental oil-pictures used the fluorescein fluid "*Robinair RA 16286B Universal A/C DYE*" mixing with ethanol as the color material. These figures show the flow structure on the sidewall. Due to the viscous effect of the flow and the friction on the sidewall, the flow velocity close to the wall is very small, thus the centrifugal force of the flow is reduced in this region. Since the static pressure is essentially the same in the boundary layer as it is in the adjacent outer flow, it is typical that streamline is curved within the boundary layer of the sidewall (on the sidewall).

The numerical and experimental oil-pictures have a good agreement. Fig. 12 shows the flow structure of blade A. The streamline moves parallel towards the blade from the inlet area with the given incidence angle (marked in red). When the inflow hits the saddle point near the leading edge of the blade, it separates into two parts. One part of the inflow moves towards the suction side of the blade (marked in orange). This flow reattaches later to the suction side of the blade. The other part of the inflow flows is curved (marked in green).

The curvature of the streamline depends on the secondary flow. The secondary flow becomes stronger with the increasing incidence. Therefore, for $i = 5^o$, the secondary flow is stronger, so the streamline is more curved and the attachment point of the separated flow (marked in orange) on the suction side of the blade moves over a short distance to the leading edge of the blade (Fig. 13).

The flow structures of blade B are similar to blade A at the same incidences. Due to the flat leading edge, the inflow of blade B separates more strongly at the saddle point near the leading edge of the blade than blade A (s. Figs. 14 and 15).

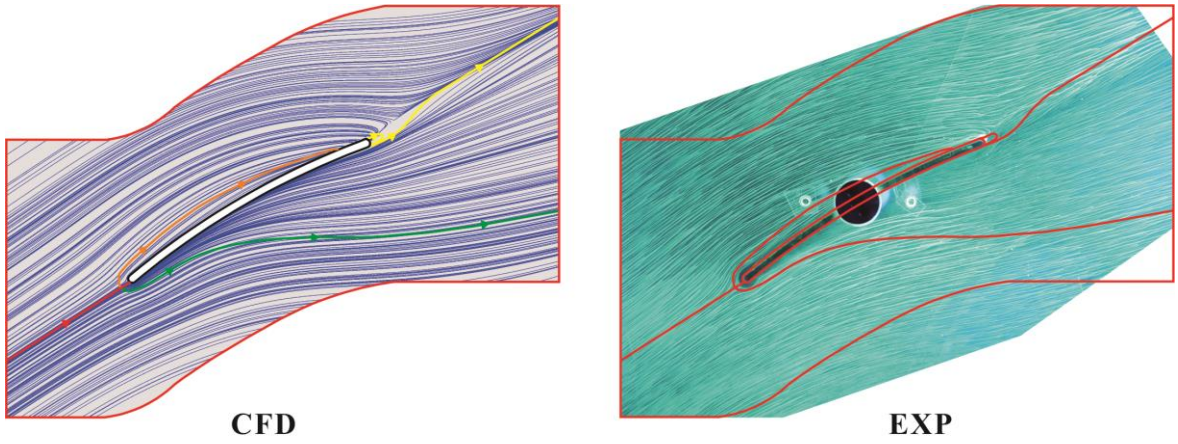

Figure 12: flow structure of blade A, i = -5°

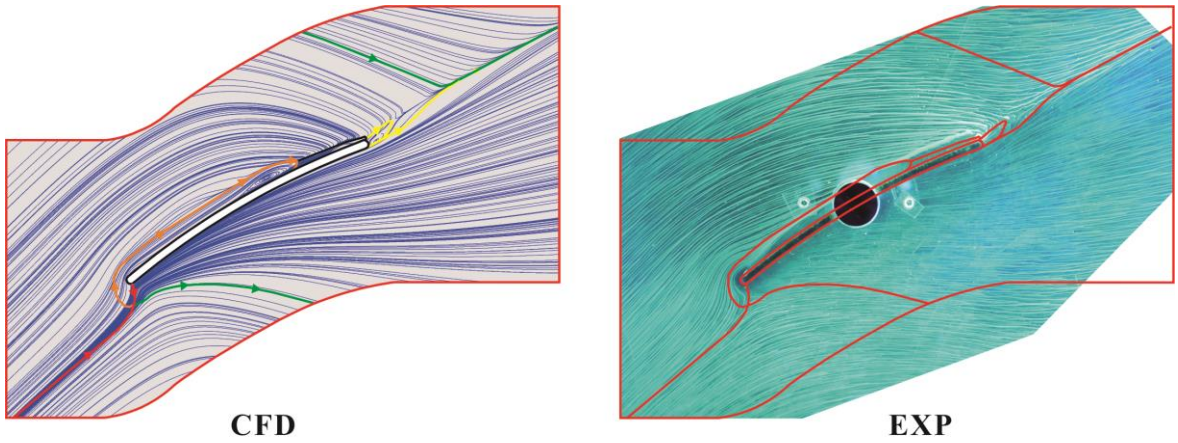

Figure 13: flow structure of blade A, i = 5°

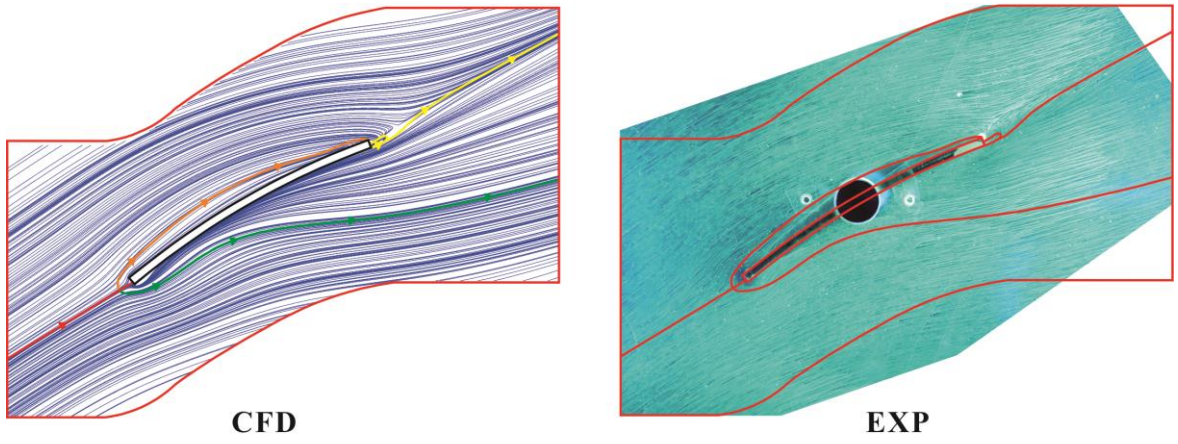

Figure 14: flow structure of blade B, i = -5°

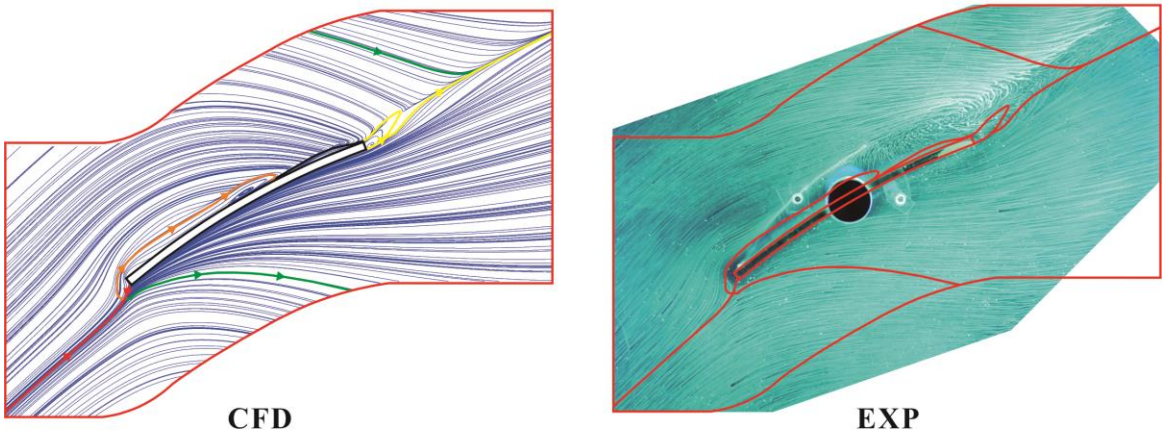

Figure 15: flow structure of blade B, i = 5^o

Separation bubbles

The main difference of blade A and blade B is the leading edge geometry, which leads to a different flow structure, especially regarding the separation bubbles at the leading edge. Based on the numerical investigation, Figs. 16 and 17 illustrates the separation bubbles of both blades for incidence i = 5^o and 5^o. In order to reduce the influence of the sidewall on the separation bubbles, the separation bubbles are investigated numerically on symmetry plane.

Due to the flat leading edge, the flow separation of blade B is stronger than blade A, which leads to the larger separation bubbles of blade B. When incidence is increasing, the separation bubbles become smaller on the pressure side of the blade and larger on the suction side of the blade.

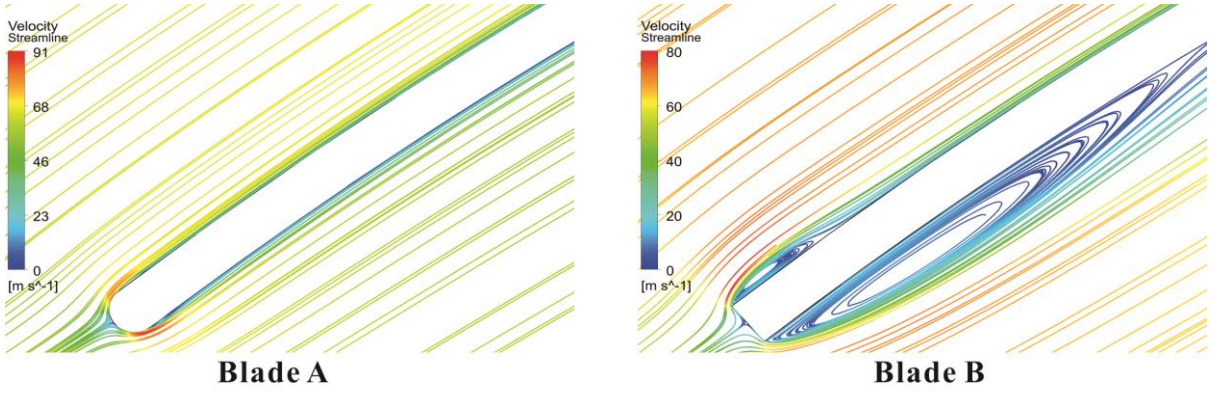

Figure 16: separation bubbles, i = - 5^o

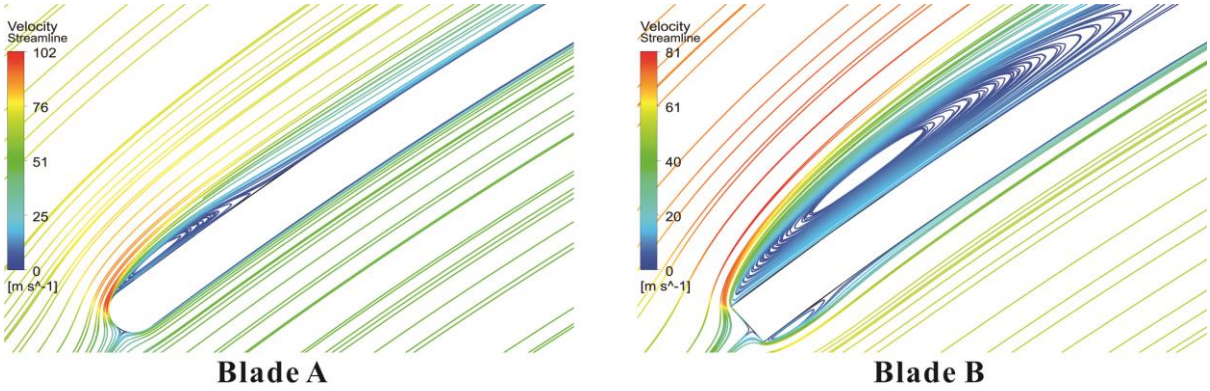

Figure 17: separation bubbles, i = 5^o

CONCLUSION

In this study, two kinds of circular arc blade with different leading edges are examined by both numerical and experimental methods to compare the flow loss and flow structure between them. As the results show, the leading edge geometry has a significant influence on the flow loss. Due to the flat leading edge, blade B has a higher flow loss than blade A. However, the variation of leading edge geometry has no significant influence on the turning angles.

Due to the friction on the sidewall and blade, high flow losses generates in the region which is near the sidewall and blade, especially in the corner between them. The loss distributions of both blades are similar in the corner between the blade and sidewall. Due to the larger flow separation of blade B, it has a larger area of high losses in the wake than blade A.

On the basis of the numerical and experimental oil-pictures, it can be clearly detected that the streamline is curved on the sidewall. When the incidence is increasing, due to the stronger secondary flow, the curvature of the streamline is also stronger. The flow structures of blade A and blade B are similar. The main difference of the flow structure between them is that blade B has stronger flow separation and larger separation bubbles at the leading edge than blade A.

BIBLIOGRAPHY

[1] Weinig, F – *The flow around blades of turbomachines*. Technical Report, **1935**

[2] John B. McDevitt, Lionel L. Levy Jr., George S. Deiwert – *Transonic Flow about a Thick Circular-Arc Airfoil,* AIAA Journal, **1976**

[3] T. Bian, Q. Han, M. Böhle – *A Design Method for Cascades Consisting of Circular Arc Blades with Constant Thickness.* International Journal of Fluid Machinery and Systems, Vol.10, **2017**

[4] T. Setoguchi, K. Kaneko – *Prediction of Cascade Performance of Circular-Arc Blades with CFD.* International Journal of Fluid Machinery and Systems, Vol.4, **2011**

[5] T. Bian, Q. Han, M Böhle – *Comparison between NACA 65 Profile and Circular Arc Blade Based on Numerical Investigation.* Proceedings of the ASME **2017** Fluids Engineering Division Summer Meeting

[6] Menter F.R., Langtry R.B., L. S. S., Y. H. P. – *A correlation-based transition model using local variables, part i - model formulation.* ASME Turbo Expo, **2004**

[7] Ansys. – *Ansys fluent user's guide release 15.0*. ANSYS Inc., **2013**.